J Mater Sci (2009) 44:794–798
DOI 10.1007/s10853-008-3139-3

Synthesis of $In(OH)_3$ and In_2O_3 nanomaterials incorporating Au

Shih-Yeh Chen · Ming-Cheng Wu · Chi-Shen Lee · M. C. Lin

Received: 31 March 2008 / Accepted: 26 November 2008 / Published online: 27 December 2008

Abstract $In(OH)_3$ and In_2O_3 nanocrystals of rectangular shape and incorporating Au were synthesized with a hydrothermal process and thermal decomposition. Powder X-ray diffraction, electron microscopy (SEM, TEM), and energy-dispersive spectroscopy studies reveal that elemental Au nanoparticles are dispersed on the surface of $In(OH)_3$ rectangular nanocrystals and incorporated into In_2O_3 nanoporous particles. UV–vis spectral measurements reveal a surface-enchanced plasma band near $\lambda \sim 532$ nm for both Au-incorporating nanomaterials. The BET surface areas of Au-incorporating $In(OH)_3$ and In_2O_3 are 26.2 and 35.5 m^2/g, respectively. The incorporation of elemental Au in $In(OH)_3$ and In_2O_3 nanomaterials is attractive for sensor, catalyst and solar-cell applications.

Introduction

Materials with confined structures have attracted much research; especially nanoporous metal oxides incorporating metallic nanoparticles that are potentially useful for applications including catalysts, photocatalysts, solar cells and sensors [1–7]. Among such reported materials, $In(OH)_3$ and In_2O_3 are of particular interest due to their peculiar physical properties: they both are wide band-gap semiconductors. A thin film of $In(OH)_3$ exhibits conductivity in a range 10^{-7}–10^{-3} S cm^{-2}, and In_2O_3 nanomaterials show satisfactory electrical conductivity and a high sensitivity towards some gases [8–10]. According to recent reports, $In(OH)_3$ and In_2O_3 nanomaterials with special shapes have been synthesized, including nanoparticles, nanocubes, nanopyramids [11], nanorods, nanowires, nanotubes, nanorod bundles, hollow microspheres, and thin films [12–19]. Metallic nanoparticles of gold are known to exhibit a deep red color, arising from surface plasmon absorption, and remarkable catalytic properties for many reactions [20]. If gold nanoparticles can be incorporated into a nanoporous metal oxide through a direct method, this composite form might improve the catalytic activity of gold nanoparticles because of the large surface area of the nanoporous metal oxide and the highly distributed metal nanoparticles; such a material would find broad applications. Several gold-modified In_2O_3 materials have been investigated, such as In_2O_3-supported gold nanoparticles as a catalyst for the epoxidation of styrene [21] and an In_2O_3/TiO_2-supported gold catalyst for oxidation of CO [22], but no report of an incorporation of Au into either $In(OH)_3$ or In_2O_3 nanomaterial has appeared. As these metal-incorporating oxide materials are prospectively applicable as nanodevices for sensors and catalysts, our research has focused on discovering new synthetic routes to deposit a metallic element on metal–oxide nanoparticles under mild conditions without a template reagent. Here we describe an approach to prepare $In(OH)_3$ and In_2O_3 nanomaterials with rectangular shapes into which elemental Au has been incorporated.

Experimental

Synthesis of $In(OH)_3$ and In_2O_3

$In(OH)_3$ nanoparticles were synthesized from $In(OH)_x$ gel under hydrothermal condition. In a typical experiment,

S.-Y. Chen · M.-C. Wu · C.-S. Lee (✉) · M. C. Lin
Department of Applied Chemistry and Institute of Molecular Science, National Chiao Tung University, 1001 University Rd, Hsinchu 30010, Taiwan, ROC
e-mail: chishen@mail.ac.nctu.edu.tw

sodium hydroxide solution (10 M, 72 mL) was added dropwise to $InCl_3$ solution (0.3 g, 1.35 mmol) under vigorous stirring at 23 °C. The milky-white colloid suspension, $In(OH)_x$ gel, was subjected to vigorous stirring and sonic treatment for at least 30 min before being transferred to a Teflon-lined stainless-steel autoclave (capacity 23 mL) and heated at 160 °C for 20 h. The white precipitate of $In(OH)_3$ was washed thoroughly with DI water under ultrasonic condition (240 W output), centrifuged and finally dried in vacuum to collect the product. Nanoporous In_2O_3 shows a light yellow color, obtained on calcination of $In(OH)_3$ in a crucible at a temperature of 450 °C and maintained in air for 2 h.

Synthesis of Au-incorporating $In(OH)_3$ and In_2O_3

In a typical experiment, a sodium hydroxide solution (72 mL, 10 M) was added dropwise to $InCl_3$ (0.3 g, 1.35 mmol) under vigorous stirring at 23 °C, followed by slow addition of $HAuCl_4$ solution (5%) until a molar ratio Au/In = 1/20. To maintain an even distribution of Au in the host $In(OH)_3$ nanocrystals, careful control of the molar ratio of Au to In and of the rate of mixing of $HAuCl_4$ solution are required. From a reaction with a molar ratio Au/In > 1/20, isolated gold nanoparticles were observed. The light yellow solution was subjected to vigorous stirring and sonic treatment for at least 30 min before being transferred to a Teflon-lined stainless-steel autoclave (capacity 23 mL) and heated at 160 °C for 20 h. The violet-red precipitate was washed thoroughly with DI water under ultrasonic conditions (output 240 W), centrifuged and finally dried in vacuum to collect the product. The powder as prepared was calcined in a crucible at temperature 450 °C and maintained for 2 h in air.

Characterization: XRD, UV, PL, SEM, TEM, TGA, BET

The product as prepared was characterized by powder X-ray diffraction (Bruker AXS D8 Advance, Leipzig Germany, CuK_α radiation at 40 kV and 40 mA), SEM (Hitachi, S-4700I, operated at 15 kV), TEM (JEOL, JEM-3000F, operated at 200 kV), UV–vis absorption spectra (Hitachi, U-3010 spectrometer, scanning wavelength 190 nm ~1,000 nm, Al_2O_3 plate as reference), thermogravimetric analyis (TGA, Perkin-Elmer Pyris, T = 50–750 °C, rate 10 °C/min), and PL measurements (Jobin-Yvon Spex Fluorolog-3, λ_{ex} = 365 nm, filter wavelength = 400 nm, Xe lamp, 23 °C, scanning wavelength 200–800 nm). Surface areas were determined by the BET method from the adsorption of nitrogen at 77 K with a surface area analyzer (NOVA 1000e-Series). The unit-cell parameters were obtained by refining the maxima of the XRD patterns with a least-squares refinement method using the CELREF program [23].

Results and discussion

With $InCl_3$ and $HAuCl_4$ as precursors under strong basic conditions ($[OH^-] \sim 10$ M), $In(OH)_3$ and In_2O_3 nanomaterials incorporating elemental gold were synthesized by a hydrothermal process and thermal decomposition. The colors of $In(OH)_3$ and In_2O_3 nanomaterials were white and yellow, respectively. Once Au nanoparticles became incorporated into these samples, a violet-red color resulted for each sample. The results indicate that gold ions were reduced to form nanoparticles and distributed within $In(OH)_3$ and In_2O_3 nanocrystals (Fig. 1a). The powder

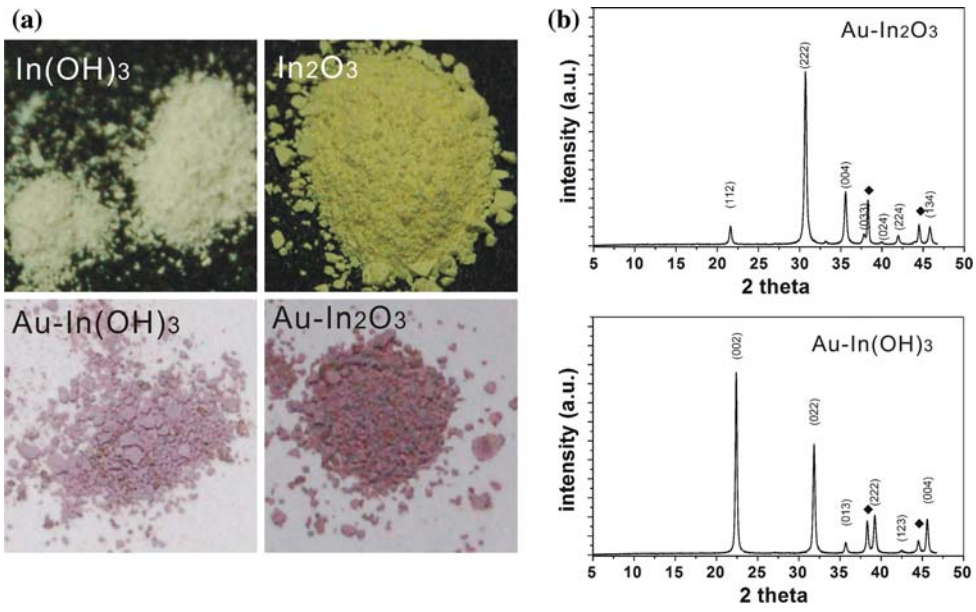

Fig. 1 **a** Colors of $In(OH)_3$, $In2O_3$, Au–$In(OH)_3$ and Au–In_2O_3 powder samples. **b** Temperature-dependent synchrotron powder-diffraction patterns of Au–$In(OH)_3$. Diffraction signals of Au are labeled with black diamonds

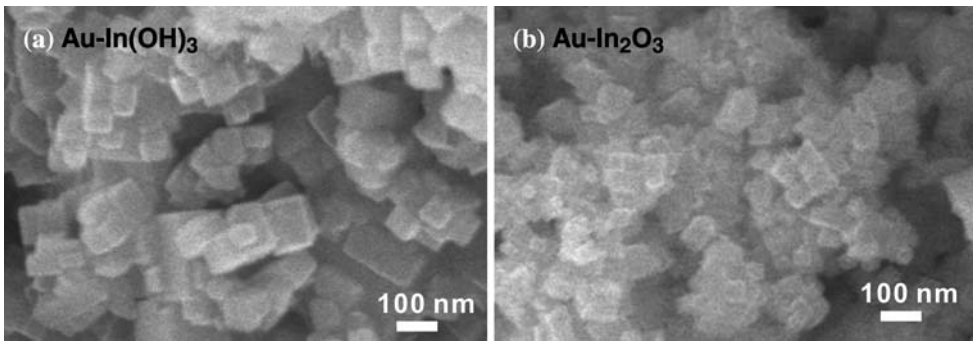

Fig. 2 SEM images of **a** Au–$In(OH)_3$ and **b** Au–In_2O_3

samples of Au incorporating $In(OH)_3$ and In_2O_3 were investigated with powder X-ray diffraction; the results appear in Fig. 1b. Broad lines attributed to Au (JCPDS Card No. 04-0784), $In(OH)_3$ (JCPDS Card No. 85-1338), and In_2O_3 (JCPDS No. 71-2195) were observed. These broad diffraction features indicate a nanocrystalline structure of Au-$In(OH)_3$ and Au-In_2O_3 samples. No crystalline impurity phase was detected with PXRD for either of the product. The diffraction patterns were indexed to cubic cells with lattice parameters $a = 7.978(2)$ Å for $In(OH)_3$ and $a = 10.116(2)$ Å for In_2O_3.

The nanomaterials as-synthesized were further characterized using scanning/transmission electron microscopy (SEM/TEM). SEM images of the Au–$In(OH)_3$ sample show nanocrystals of rectangular shape with average edge length of 60 nm (Fig. 2a). After complete decomposition at 450 °C, the overall morphology of Au–In_2O_3 shows no significant alteration (Fig. 2b). According to X-ray energy-dispersive spectroscopy (EDS), only a small proportion of elemental gold ($\sim$1% at.) was deposited on the surface of the $In(OH)_3$ nanocrystals. For reaction with a molar ratio of Au:In = 1:20, the product shows an unevenly distributed violet-red color, indicative of more isolated Au nanoparticles being produced. With a transmission electron microscope (TEM) to investigate the fine structure of $In(OH)_3$/In_2O_3 samples, Fig. 3a shows a TEM image of an $In(OH)_3$ single crystal of rectangular shape. The selected-area electron diffractions (SAED) exhibit a [001] zone-axis diffraction of bcc $In(OH)_3$ (inset of Fig. 3a), indicative of a single-crystalline product; small holes on the surface are due to defects during the growth of this single crystal. A TEM image of an In_2O_3 particle in Fig. 3b notably exhibits a rectangular shape with a highly porous morphology formed by interconnected indium-oxide nanocrystals with an average pore diameter of $\sim$5 nm. The wall thickness is about 5 nm for most aggregated rectangular nanoporous samples. The fine structure of a small domain exhibits a lattice fringe of spacing 0.29 nm, in agreement with the *d* value of (222) planes of the cubic In_2O_3 structure. The SAED pattern revealed a pattern of rings and dots that is indexed to cubic In_2O_3, indicative of the polycrystalline

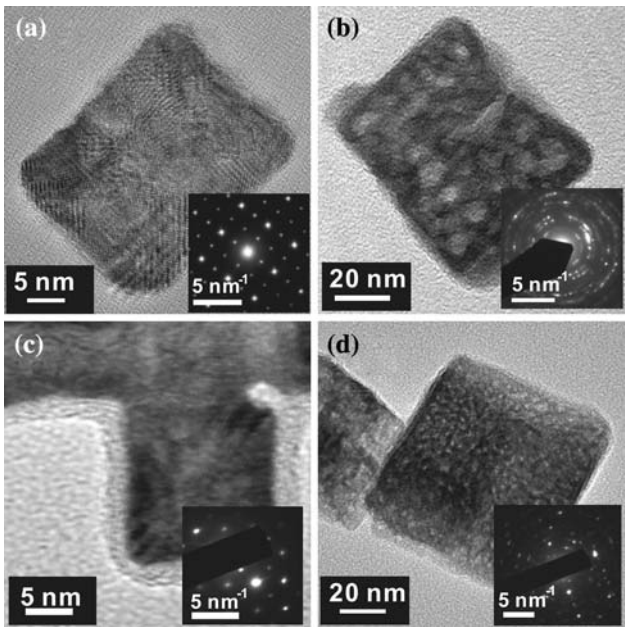

Fig. 3 TEM images and corresponding SAED patterns (insets) of **a** $In(OH)_3$, **b** In_2O_3, **c** Au–$In(OH)_3$, and **d** Au–In_2O_3

nature of the nanoporous In_2O_3. Figure 3c shows a TEM image from an Au-incorporating $In(OH)_3$ single crystal that is covered with a thin film of elemental gold (thickness $\sim$1 nm) confirmed by TEM–EDS area-mapping analysis. When Au is incorporated into this nanoporous In_2O_3 material, the shape of the nanoporous Au–In_2O_3 is essentially the same as for the In_2O_3 product, but the average pore diameter is decreased to $\sim$1.0 nm; this form is unprecedented for an indium-oxide nanostructure. No indication of a thin film similar to Au–$In(OH)_3$ was found in the Au–In_2O_3 sample. EDS measurements on nanoporous Au–In_2O_3 show the existence of elemental Au, In and O. TEM–EDS area-mapping analysis for elemental Au shows a scattered distribution of an Au signal, indicating that elemental Au was incorporated into the nanoporous In_2O_3 host material. The data indicate that the Au nanoparticles on the surface of an $In(OH)_3$ nanocrystal were transferred into the cavities of nanoporous In_2O_3 nanoparticles. The BET surface area for the as-synthesized $In(OH)_3$

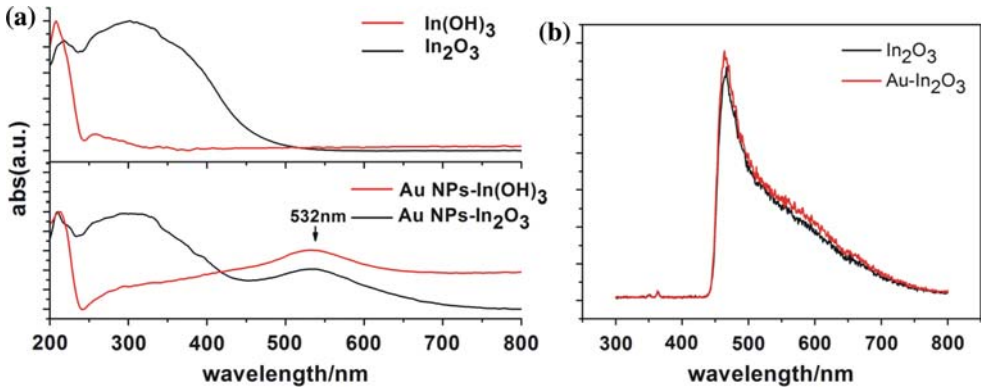

Fig. 4 **a** UV–vis diffuse reflectance spectra of Au–$In(OH)_3$ and Au–In_2O_3. **b** Photoluminescence (PL) spectra of In_2O_3 and Au–In_2O_3 powders ($\lambda_{ex} = 365$ nm)

and In_2O_3 nanomaterials area 23.5 and 37.4 m^2/g, while the surface area for the Au-incorporated slightly change to 27 m^2/g for Au–$In(OH)_3$ and 35.5 m^2/g for Au–In_2O_3. The surface area of nanoporous In_2O_3/Au-In_2O_3 is higher than that of $In(OH)_3$/Au-$In(OH)_3$ nanoparticles, indicative of the formation of porous structure in In_2O_3 sample. The surface area of Au–$In(OH)_3$ is slightly higher than $In(OH)_3$, while the surface area of nanoporous In_2O_3 is less than Au–In_2O_3. The BET results for these samples show small differences, which suggests weak effect of Au nanoparticles to the measured surface area of Au-incorporated samples.

Visible diffuse reflection spectra of both Au-incorporating samples clearly show an intense absorption maximum about 532 nm, attributed to the surface–plasma excitation of gold nanoparticles (Fig. 4a) [24]. The band gaps of $In(OH)_3$ and In_2O_3 host materials are calculated to be 5.57 and 3.74 eV, respectively, which are similar to reported values[25]. Photoluminescence (PL) spectra of both In_2O_3 and Au–In_2O_3 nanoporous materials show a PL emission in the blue-green region with its maximum intensity centered at 467 nm (Fig. 4b); this emission is attributed to a radiative recombination of a photo-excited hole with an electron occupying oxygen vacancies in the In_2O_3 host, analogous to the PL mechanism of ZnO defect nanocrystals [26, 27]. During the thermal decomposition, oxygen vacancies are expected to be generated at a large concentration in nanoporous In_2O_3 because of O and H bonds released when In_2O_3 begins to form. Similar PL spectra with maxima in the blue-green region are reported for In_2O_3 nanoparticles [12], nanocubes [28, 29], and nanofibers [30].

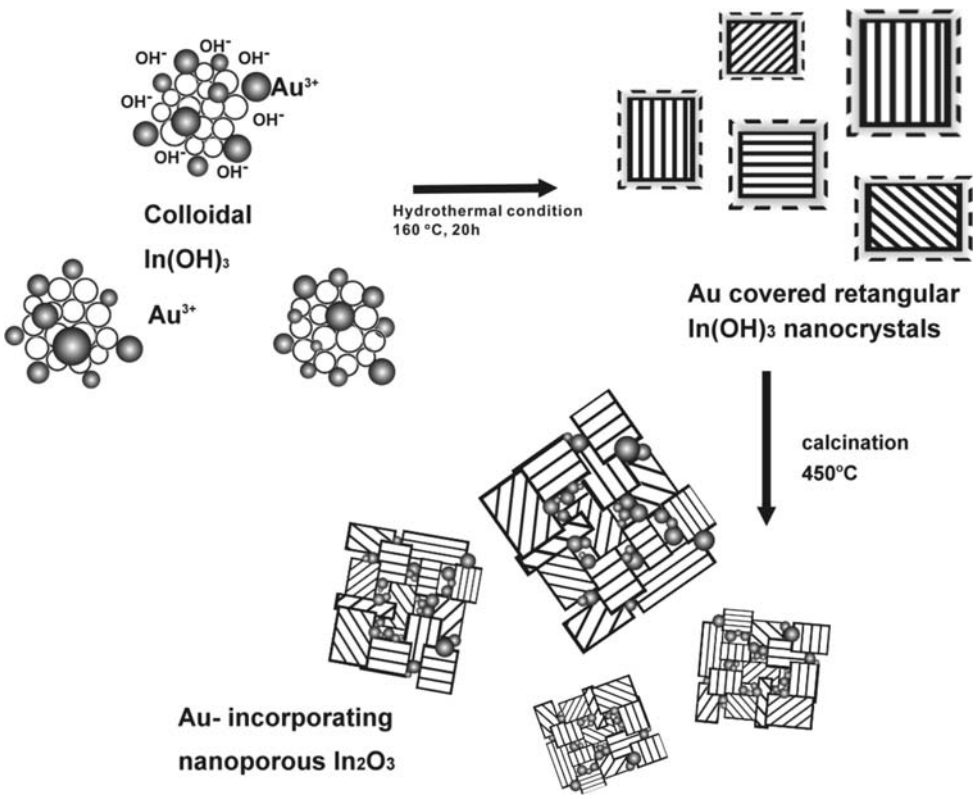

Fig. 5 Schematic illustration of the transformation of an Au-incorporating indium hydroxide rectangular nanocrystal to a nanoporous indium-oxide of rectangular form through a hydrothermal process and thermal decomposition

According to the experimental observations we propose a mechanism for the formation of the Au-incorporating nanomaterials. As illustrated in Fig. 5, $Au(OH)_4^-$ complexes are initially attached at the surface of $In(OH)_3$ colloids during the hydrothermal process [31]. The Au^{3+} ions become subsequently reduced by chloride ion under basic conditions according to this reaction:

$$2Au^{3+} + 3Cl^- + 6OH^- \rightarrow 2Au + 3ClO^- + 3H_2O$$

This reduced elemental Au covers the surface of $In(OH)_3$ nanocrystals. During thermal decomposition, the newly formed indium-oxide begins to form on the surface of $In(OH)_3$. H_2O molecules are released within the $In(OH)_3$ nanocrystal and cause the formation of small voids or pores until indium hydroxide is completely decomposed to form nanoporous indium-oxide. The Au nanoparticles become transferred into the pores or interstitial regions of nanoporous In_2O_3. This proposed mechanism indicates that gold ions become reduced to gold nanoparticles with a hydrothermal method and precursor $HAuCl_4$ in a strongly basic solution, which has been confirmed by experiments.

Conclusion

$In(OH)_3$ and In_2O_3 nanocrystals of rectangular shape and incorporating Au nanoparticles have been prepared using a hydrothermal reaction followed by thermal decomposition. This method provides a route to synthesize Au-incorporating $In(OH)_3$ and In_2O_3 nanostructures with a well controlled internal structure. This procedure is readily generalizable to prepare other metal-incorporating nanoporous metal–oxide materials; such Au-incorporating nanomaterials are expected to serve as catalyst, gas sensor, and quantum-dot solar-cell substrate. Such applications are currently under investigation.

Acknowledgements For technical assistance we thank Dr. Hwo-Shuenn Sheu at National Synchrotron Radiation Research Center for the XRD experiment, Professors Jim Leu and Chia-Ming Yang for BET measurements, Professor Teng-Ming Chen for UV and PL measurements and Professor Chain-Shu Hsu for TGA measurements. Institute of Nuclear Energy Research, Atomic Energy Council, Taiwan (contract NL940251) and National Science Council (contracts NSC94-2113-M-009-012, 94-2120-M-009-014) supported this research. MCL acknowledges Taiwan Semiconductor Manufacturing Co. for the TSMC distinguished professorship and Taiwan National Science Council for the Distinguished Visiting Professorship at National Chiao Tung University.

References

1. Li J, Hao J, Cui X, Fu L (2005) Catal Lett 103:75
2. Gervasini A, Perdigon-Melon JA, Guimon C, Auroux A (2006) J Phys Chem B 110:240
3. Hsiao WI, Lin YS, Chen YC, Lee CS (2007) Chem Phys Lett 441:294
4. Lei Z, Maa G, Liu M, You W, Yan H, Wu G, Takata T, Hara M, Domen K, Li C (2006) J Catal 237:322
5. Tian Y, Tatsuma T (2005) J Am Chem Soc 127:7632
6. Chen X, Mao SS (2007) Chem Rev 107:2891
7. Zuruzi AS, MacDonald NC, Moskovits M, Kolmakov A (2007) Angew Chem Int Ed 46:4298
8. Ishida T, Kuwabara K (1998) J Ceram Soc Jpn 106:381
9. Li C, Zhang D, Lei B, Han S, Liu X, Zhou C (2003) J Phys Chem B 107:12451
10. Soulantica K, Erades L, Sauvan M, Senocq F, Maisonnat A, Chaudret B (2003) Adv Funct Mater 13:553
11. Datta A, Panda SK, Ganguli D, Mishra P, Chaudhuri S (2007) Cryst Growth Design 7:163
12. Liu Q, Lu W, Ma A, Tang J, Lin J, Fang J (2005) J Am Chem Soc 127:5276
13. Huang J, Gao L (2006) Cryst Growth Design 6:1528
14. Wang G, Park J, Wexler D, Park MS, Ahn J-H (2007) Inorg Chem 46:4778
15. Li C, Zhang D, Han S, Liu X, Tang T, Zhou C (2003) Adv Mater 15:143
16. Du N, Zhang H, Chen B, Ma X, Liu Z, Wu J, Yang D (2007) Adv Mater 19:1641
17. Yang J, Lin C, Wang Z, Lin J (2006) Inorg Chem 45:8973
18. Li B, Xie Y, Jing M, Rong G, Tang Y, Zhang G (2006) Langmuir 22:9380
19. Basharat S, Carmalt CJ, Barnett SA, Tocher DA, Davies HO (2007) Inorg Chem 46:9473
20. Daniel M-C, Astruc D (2004) Chem Rev 104:293
21. Patil NS, Jha R, Uphade BS, Bhargava SK, Choudhary VR (2004) Appl Catal A Gen 275:87
22. Debeila MA, Wells RPK, Anderson JA (2006) J Catal 239:162
23. Laugier J, Bochu B (2003) CELREF. Laboratoire des Matèriaux du Genie Physique, Saint Martin d'Hères, France
24. Daniel M-C, Astruc D (2004) Chem Rev 104:293
25. Zhuang Z, Peng Q, Liu J, Wang X, Li Y (2007) Inorg Chem 46:5179
26. Özgür Ü, Alivov YI, Liu C, Teke A, Reshchikov MA, Doğan S, Avrutin V, Cho S-J, Morkoçd H (2005) J Appl Phys 98:041301
27. Wu M-C, Lee C-S (2006) Inorg Chem 45:1415
28. Lee CH, Kim M, Kim T, Kim A, Paek J, Lee JW, Choi S-Y, Kim K, Park J-B, Lee K (2006) J Am Chem Soc 128:9326
29. Tang Q, Zhou W, Zhang W, Ou S, Jiang K, Yu W, Qian Y (2005) Cryst Growth Design 5:147
30. Liang CH, Meng GW, Lei Y, Phillipp F, Zhang LD (2001) Adv Mater 13:1330
31. Baes CF, Mesmer RE (1986) The hydrolysis of cations. R.E. Krieger, Malabar, Fla